In vivo modulation of morphogenetic movements in *Drosophila* embryos with femtosecond laser pulses

Willy Supatto*, Delphine Débarre†, Bruno Moulia‡, Eric Brouzés*, Jean-Louis Martin†, Emmanuel Farge*, and Emmanuel Beaurepaire†§

*Mechanics and Genetics of Developmental Embryology, Centre National de la Recherche Scientifique, Unité Mixte de Recherche 168, Curie Institute, 11 Rue Pierre et Marie Curie, F-75005 Paris, France; †Laboratory for Optics and Biosciences, Centre National de la Recherche Scientifique, Unité Mixte de Recherche 7645, Institut National de la Santé et de la Recherche Médicale U696, Ecole Polytechnique, F-91128 Palaiseau, France; and ‡Biomechanics Group, Institut National de la Recherche Agronomique, Unité Mixte de Recherche 547, 234 Avenue du Brézet, F-63039 Clermont-Ferrand, France

Edited by Kathryn V. Anderson, Sloan–Kettering Institute, New York, NY, and approved November 30, 2004 (received for review July 22, 2004)

The complex biomechanical events associated with embryo development are investigated *in vivo*, by using femtosecond laser pulse-induced ablation combined with multimodal nonlinear microscopy. We demonstrate controlled intravital ablations preserving local cytoskeleton dynamics and resulting in the modulation of specific morphogenetic movements in nonmutant *Drosophila* embryos. A quantitative description of complex movements is obtained both in GFP-expressing systems by using whole-embryo two-photon microscopy and in unlabeled nontransgenic embryos by using third harmonic generation microscopy. This methodology provides insight into the issue of mechano-sensitive gene expression by revealing the correlation of *in vivo* tissue deformation patterns with Twist protein expression in stomodeal cells at gastrulation.

femtosecond pulse-induced ablation | two-photon microscopy | third-harmonic generation microscopy | *Drosophila* gastrulation

Investigating the complex dynamical processes involved in embryo development, from gene expression to morphogenesis, remains a challenging area in biology at the crossing of genetics, cell biology, biomechanics, and tissue imaging (1, 2). Embryo development involves a complex choreography of cell movements initiated at gastrulation that are highly regulated both in time and space. The genetic control of morphogenetic movements shaping the embryo is extensively studied, particularly in *Drosophila melanogaster*, which provides a major model of developmental genetics (3). On the other hand, the influence of mechanical factors in development was recently pointed out. It was proposed that hemodynamic forces participate in the control of cardiogenesis in Zebrafish embryos (4), and that tissue deformations associated with morphogenetic movements are involved in modulating developmental gene expression during *Drosophila* gastrulation (5). The genetic regulation of morphogenesis is generally investigated by taking advantage of mutants exhibiting disrupted morphogenetic movements. Similarly, the mechanical regulation of morphogenesis could be directly addressed by modifying the mechanical integrity of wild-type embryos in a nongenetic manner, such as by using intravital laser ablations. Indeed, recent studies reported that tight focusing of nanojoule femtosecond near-infrared laser pulses inside *ex-vivo* biological tissues can induce 3D-confined submicrometer ablations (6), owing to the nonlinear nature of ultrashort pulse interactions with matter (7, 8). This approach was recently used *in vitro* for targeted cell transfection (9).

Combining nonlinear microscopies [two-photon excited fluorescence (2PEF) (10) and third-harmonic generation (THG) (11)] and femtosecond pulse-induced ablation, we succeeded in modulating, visualizing, and quantifying morphogenetic movements in nonmutant *Drosophila* embryos. To begin, we demonstrate that femtosecond laser pulse-induced ablation ("multiphoton ablation") makes it possible to perform controlled, 3D-confined intravital microdissections within developing embryos, without significantly perturbing cytoskeleton dynamics around ablated areas. In turn, localized tissue ablations can be used for the controlled long-distance modulation of specific morphogenetic movements during gastrulation. In addition, we show that the same laser source can be used to quantitatively analyze native and disrupted morphogenetic movements *in vivo*. Long-term 2PEF whole-embryo imaging of transgenic GFP-expressing strains permits a direct understanding of movements in space and their automated micrometer description through velocimetric image analysis. This methodology is applied to the study of mechano-sensitive gene expression (5) by correlating cell movements with the pattern of gene expression. Finally, we generalize our approach to the quantified modulation of morphogenetic movements in unlabeled nontransgenic embryos by extending THG microscopy to the visualization of morphogenetic movements, and demonstrating its straightforward combination with multiphoton ablation.

Methods

Embryo Preparation. Oregon-R was used as the wild-type *D. melanogaster* strain. Transgenic flies containing eGFP fused with a nuclear localization sequence (nls-GFP, Bloomington Stock Center, Indiana University) exhibit a strong fluorescent labeling of nuclei (12). The sGMCA transgenic line (13) expresses eGFP fused with actin-binding moesin fragments [gift from D. P. Kiehart and R. A. Montague (Duke University, Durham, NC)] and provides a fluorescent outline of cell shape. Embryos were collected during cellularization at developmental stage 5 (stages defined in ref. 14), dechorionated, and glued to a coverslip. During laser microdissection and image acquisition, embryos were maintained in PBS at room temperature (19 ± 1°C). Large working distance objectives were used to prevent hypoxia.

Nonlinear Microscopy and Ablations. Imaging and ablations were performed on a custom-built nonlinear microscope incorporating a femtosecond titanium:sapphire (Ti:S) oscillator (Coherent, Santa Clara, CA), an optical parametric oscillator (OPO, APE, Berlin), galvanometer mirrors (GSI Lumonics, Billerica, MA), water-immersion objectives (0.9 N.A., Olympus, Tokyo), and photon-counting photomultipliers (Electron Tubes, Ruislip, England). A motorized beam attenuator allowed injection of up to 90% of the Ti:S beam either into the OPO for THG imaging, or directly into the microscope for ablations. 2PEF was epidetected when exciting GFP-expressing embryos at 920 nm. Alternatively, THG was detected in the transmitted direction when exciting unlabeled embryos at 1,180 nm. In either case, the signal was selected by using appropriate filters (Chroma Technology, Rockingham, VT). Because ablation efficiency was found to be nearly wavelength-

This paper was submitted directly (Track II) to the PNAS office.

Abbreviations: 2PEF, two-photon excited fluorescence; THG, third-harmonic generation; PIV, particle image velocimetry; CFI, cellularization front invagination; SP, stomodeal primordium.

§To whom correspondence should be addressed. E-mail: emmanuel.beaurepaire@polytechnique.fr.

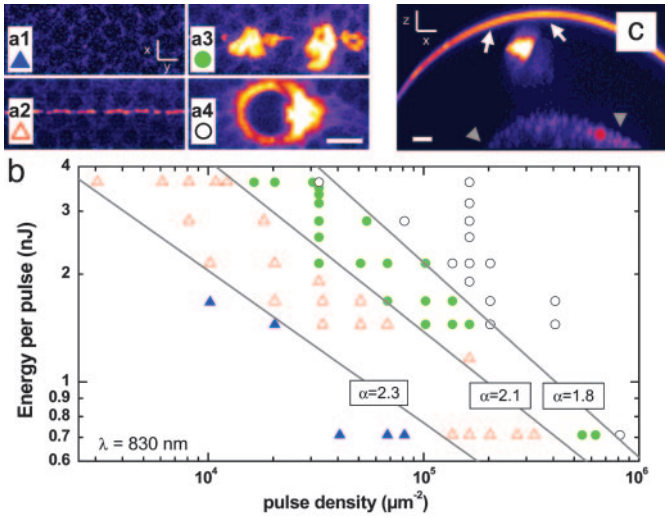

Fig. 1. Femtosecond pulses allow 3D-confined processing of embryo tissue. (*a1–a4*) Illustration of the graded effects induced inside embryos by line scans of increasing pulse energies. (*b*) Diagram of the effects induced along a 100-μm-long line scan as a function of energy per pulse and pulse density, according to the four graded regimes illustrated in *a1–a4*. Regime 1 (*a1*, filled triangles) corresponds to no detectable disruption (when monitored by using endogenous 2PEF). Regime 2 (*a2*, open triangles) corresponds to the appearance of bright fluorescence along the scan, and the onset of microexplosions in the perinuclear region of the cytoplasm. Regime 3 (*a3*, filled circles) corresponds to the occurring of cavitation bubbles lasting <5 s and creating lesions on the order of cell size (≈5–6 μm). Regime 4 (*a4*, open circles) corresponds to the formation of large bubbles (>5–6 μm) lasting >5 s. Fourteen different embryos were used to generate the diagram, and several points were recorded for each embryo. Gray lines along which the induced effect is constant represent the frontiers between regimes, and α values reflect the dependence of effects on excitation intensity ($-1/\alpha$ being the slope of the line). (*c*) Transverse view of a wild-type embryo after microdissection performed at the limit between regimes 3 and 4. The area of the vitelline membrane, which was in the path of the ablating beam (between white arrows), is left intact. (Scale bars: 10 μm.) See Movie 1.

independent over the range 830–920 nm, combined ablation/GFP imaging experiments were performed at 920 nm to optimize GFP excitation (15). Microdissections (100 μm × 40 μm) typically consisted of three line scans (100 μm long, 10–20 μm away from the vitelline membrane) performed in three successive planes separated 10–15 μm from one another. Surface-rendered 3D reconstructions were performed offline by using VOLUMEJ (M. Abramoff, University of Iowa, Iowa City).

Velocimetric Analysis. Velocimetric estimation of morphogenetic movements was performed by particle image velocimetry (PIV) analysis (16). Images (0.5 μm per pixel) were recorded every 30 or 60 s and analyzed by using the MATPIV software package (J. K. Sveen, University of Oslo, Oslo). The mean 2D deformation field (mean area strain rate) was estimated by computing the divergence of the velocity field, which provided a qualitative description of the time-dependent deformation patterns.

1D-kymograph analysis for monitoring the rate of cellularization front invagination (CFI) was performed by using METAMORPH (Universal Imaging, Downingtown, PA). Kymographs were computed along the apicobasal axis over 10 μm-wide areas, which gave a typical precision of 0.05 μm/min.

Twist Immunostaining. Embryos were fixed at stage 7 over a period of 30 min at the interface of a heptane/4% formaldehyde Pipes. Antibody staining was done in PBT (Pipes/0.2% Tween/1% BSA). Proteins were detected with rabbit anti-Twist (a gift from S. Roth, Cologne University, Cologne, Germany). FITC secondary antibody was purchased from Vector Laboratories. Embryos were mounted in Vectashield (Vector Laboratories) for observation.

Results and Discussion

Intravital Processing of Embryo Tissue Using Femtosecond Pulses. Modifying the embryo structural integrity requires performing large (several μm) controlled intravital dissections that preserve the vitelline membrane surrounding the embryo. We characterized the effects of femtosecond pulses on developing embryos at the cellular blastoderm stage (Stage 5). Pulse trains (830 nm, 76 MHz) were

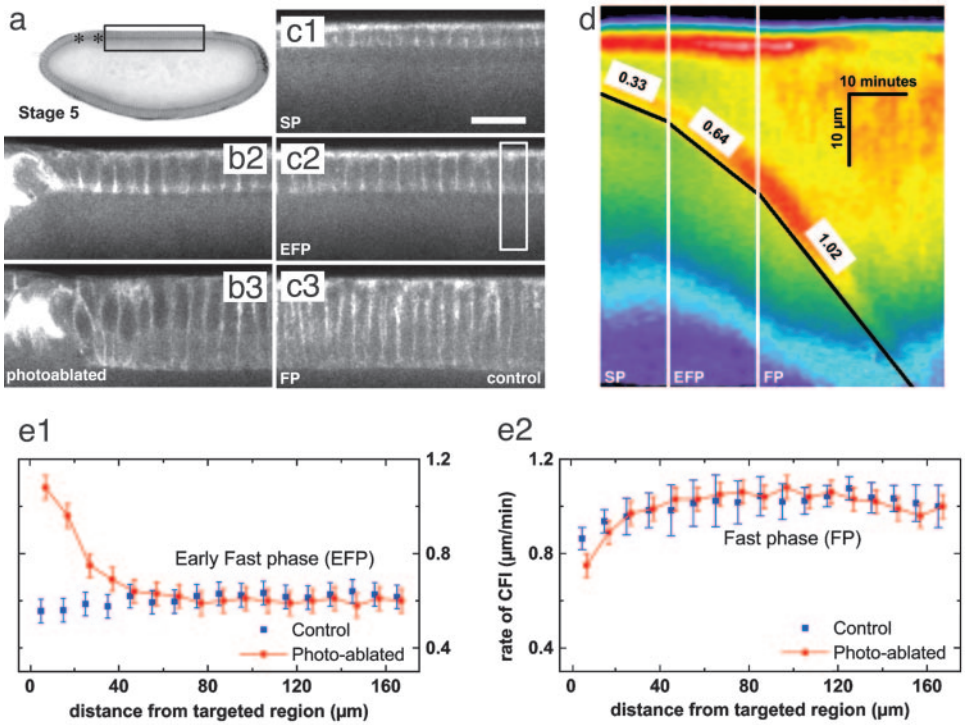

Fig. 2. Ablations induce minimal perturbation to local cytoskeleton dynamics. (*a*) sGMCA embryo before photoablation. Anterior right, dorsal up. Asterisks indicate the ablation region. (*b2* and *b3*) CFI in an sGMCA embryo near the ablation (photoablated).(*c1–c3* and *d*) Control. (*c1–c3*) CFI in an intact sGMCA embryo. (*d*) Kymograph computed along the apicobasal axis in the rectangle region in *c2*, on which the slopes at the cellularization front (black lines) directly give the CFI rate. CFI in a control embryo consisted of three phases: a slow phase (SP *Left*, ≈0.3 μm/min at 19°C), an early fast phase (EFP *Center*, ≈0.6 μm/min), and a fast phase (FP *Right*, ≈1 μm/min) after the cellularization front passes above the nuclei (21, 22). (*e1* and *e2*) Kymograph analysis. (*e1*) CFI rate measured 1 min after ablation (during EFP, solid line) at different distances from the ablated region, and comparison with control embryos (squares, $n = 3$). (*e2*) Same measurement 15 min after photoablation (during FP). (Scale bar: 20 μm.)

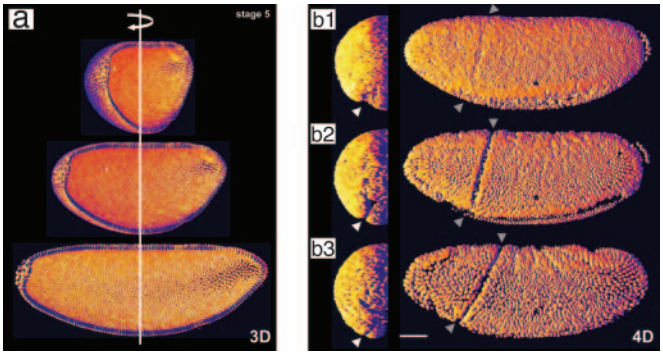

Fig. 3. Whole-embryo imaging of morphogenetic movements. (*a*) 3D reconstruction of the spatial distribution of nuclei within an nls-GFP embryo at stage 5 of development, calculated from a 2PEF XYZT stack. Rotation was through the dorsoventral axis. Fifty-five frames with 2-μm spacing were acquired, revealing the ≈3,000 nuclei of a half-embryo. (*b1–b3*) 4D imaging of a developing nls-GFP embryo. These data are extracted from a sequence of 3D images (*b1*, 4 min; *b2*, 20 min; *b3*, 36 min after the onset of gastrulation) spanning stages 5 to 7 of development, and illustrate major morphogenetic movements of gastrulation such as cephalic furrow formation [between gray arrows, lateral view (*Right*)] and ventral furrow invagination [white arrows, anterior view (*Left*)]. The embryo is slightly tilted so that the ventral furrow is visible. (Scale bar: 50 μm.) Total acquisition time: 1 min per 3D image. (See Movie 2.)

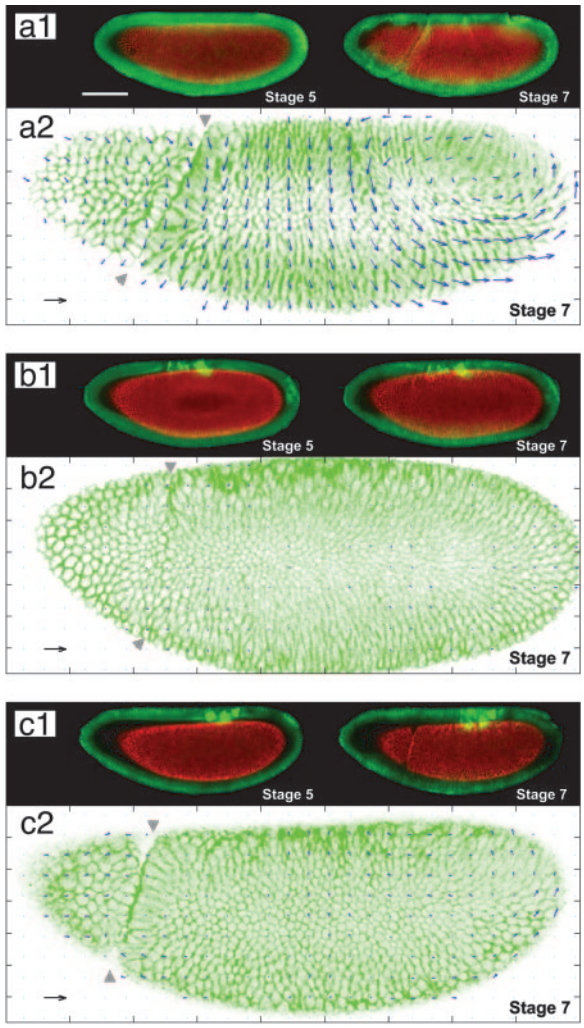

Fig. 4. Multiphoton ablation allows quantified modulation of specific morphogenetic movements (*a1* and *a2*, control; *b1* and *b2*, middorsal ablation; *c1* and *c2*, postdorsal ablation). (*a1*) Development of an intact sGMCA embryo. Green represents images recorded at the equator. Red represents images recorded ≈20 μm under the surface. (*b1*) Development of a sGMCA embryo after a 100 μm × 40 μm middorsal ablation (see *Quantified Modulation of Morphogenetic Movements* in Vivo), resulting in disrupted lateral cell movements and no cephalic furrow formation (gray arrowheads). (*c1*) Development of an sGMCA embryo after a 100 μm × 40 μm postdorsal ablation resulting in disrupted lateral cell movements only. (*a2*, *b2*, and *c2*) Corresponding velocimetric analysis for the same embryos at stage 7. Each experiment was reproduced on five different embryos and gave similar results. (Scale bar: 100 μm.) Black scale arrow, 5 μm/min.

focused 5–15 μm beneath the vitelline membrane of live wild-type embryos. Line scans were performed for different values of the energy per pulse E_{pulse} and the pulse surface density d_{pulse} (number of pulses received per surface unit), which are related to the laser average power and the scanning speed, respectively. The effect of each scan was immediately observed by attenuating the laser power and recording 2PEF images of the endogenous fluorescence around the ablation. Pulse effects were qualitatively grouped into graded regimes illustrated in Fig. 1*a*. Successive ablation patterns were defined by the appearance of intense fluorescence in perinuclear regions along the scan [which is likely related to the destruction of mitochondria (17)], and by the formation of optical breakdown-induced cell-size cavitation bubbles (6). As summarized in Fig. 1*b*, these regimes were repeatedly observed for given experimental parameters, which enabled us to perform controlled intravital microdissections. We note that inner tissue dissection requires an increase in laser power with depth according to embryo optical properties, to compensate for laser light scattering. Because embryos become more transparent as they develop, the ablation maximum depth depends on the developmental stage. At stage 5, penetration is hampered by the highly scattering nature of the yolk periphery, and micrometer-size bubbles (Fig. 1*a3*) could be induced up to only 70 μm under the surface. At embryonic development completion (stage 16), similar effects could be obtained up to 100 μm under the surface (i.e., further than the embryo equator). In the log-log representation of Fig. 1*b*, the frontiers between graded effects provide an indication of the dependence of ablations on pulse intensity. Consistent with recent studies on photodamage in two-photon microscopy(18, 19), we found that these frontiers are characterized by slopes close to $-1/2$, indicating that photodamage bears a linear dependence on pulse density and a nearly quadratic dependence on pulse energy in the conditions investigated here. Fig. 1*c* illustrates the 3D confinement of the microdissections resulting from the nonlinear process. In particular, it is possible to perform microdissections a few μm under the vitelline membrane without damaging it (See Movie 1, which is published as supporting information on the PNAS web site). Because the integrity of the vitelline membrane must be preserved to ensure early embryo viability, the ability to perform 3D-confined intravital ablations is a decisive advantage in *Drosophila* studies. More generally, these data illustrate that inner tissues can be processed in a living organism while keeping the surface intact.

Cytoskeleton Dynamics as a Probe of the Local Perturbation Induced by Multiphoton Ablation. It is expected that femtosecond pulses allow local tissue processing with limited thermal energy transfer to the surrounding areas (8). Recent *ex vivo* studies of microjoule-pulse-induced ablation in brain tissue found that regions adjacent to the targeted area exhibited no alteration of tissue physical integrity or antigenic response (20). We evaluated *in vivo* the biological perturbation induced by high repetition rate nanojoule pulses to the tissue surrounding the ablated area by monitoring the process of cellularization in developing embryos. This process is a critical and temperature-sensitive dynamical event of embryonic cells that occurs at the cellular blastoderm stage during the hour

BIOPHYSICS

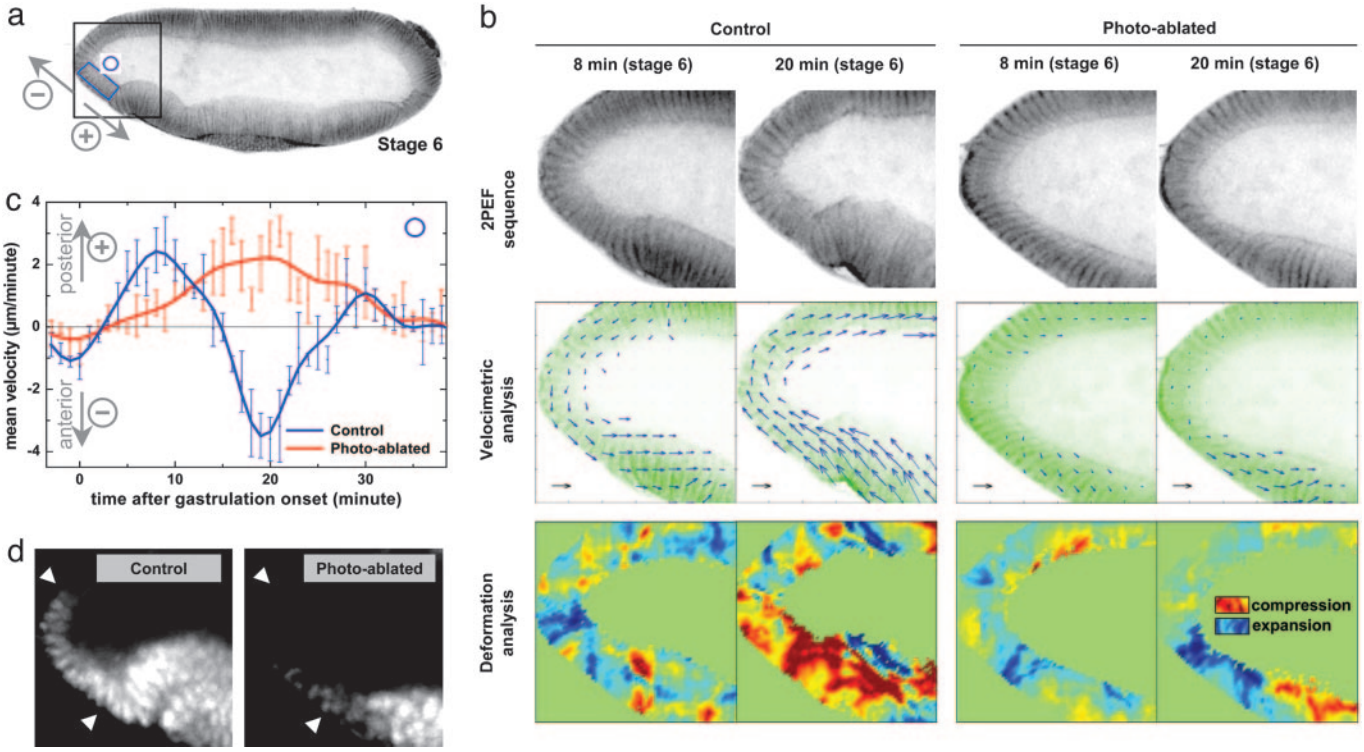

Fig. 5. Middorsal ablation modulates morphogenetic movements at the anterior pole, which are correlated with Twist expression. (*b*) Sequence of development at the anterior pole (black square region in *a*) of control and photoablated sGMCA embryos, showing the disrupted movements of SP cells after middorsal ablation (see Fig. 4*b*). Approximate time after the onset of gastrulation is indicated in minutes (inverted contrast images). (Black scale arrow: 2 μm/min.) (*c*) Mean velocity of morphogenetic movements occurring in the blue box area in *a* for both embryos. Velocity fields are projected in the direction perpendicular to the apicobasal axis of SP cells, with the convention of positive velocities toward the posterior pole (see direction arrows). Velocimetric analysis provides a quantitative description of the local modulation of morphogenetic movements resulting from the ablation. In particular, the backward/forward movement of SP tissue is disrupted, which is confirmed by the deformation analysis (divergence) of the velocity field. (*d*) *twist* expression pattern at stage 7 in an intact embryo and after middorsal ablation. Femtosecond pulse-induced disruption of SP mechanical deformations is correlated with a decrease of *twist* expression level in SP cells (between white arrows). Shown are lateral views, with anterior left and dorsal up.

preceding gastrulation. It involves oocyte plasma membrane folding between nuclei, subsequently partitioning off each nucleus in a single cell. The rate and completion of CFI appear as sensitive indicators of the integrity of cytoskeleton dynamics (21, 22). We measured that the rate of CFI in intact embryos is roughly doubled at 25°C compared with 19°C room temperature. We then performed ablations centered 10–20 μm away from the vitelline membrane in sGMCA embryos (13), and monitored cellularization around ablated regions by kymograph analysis ($n = 8$, Fig. 2). Our experiments showed that cellularization was still completed in cells adjacent to the targeted area (Fig. 2 *b* and *c*). The rate of CFI was slightly accelerated over a limited distance (40 μm corresponding to seven to eight cells) and time ($\approx$10 min) (Fig. 2 *e1* and *e2*). Three factors may account for this local perturbation: metabolism changes (17), heating (23, 24), and perturbed integrity of the supracellular cytoskeleton network (22), resulting in alterations of its mechanical state. When performing ablations close ($<$10 μm) to the membrane, we sometimes observed a local decrease of the CFI rate (not shown) apparently due to tissue fragments bound to the vitelline membrane, which indicate that the mechanical coupling between adjacent cells is a principal factor in the local perturbation. In all cases, cellularization was completed, and its rate returned to normal in $<$15 min in cells immediately adjacent to the ablated volume, thus establishing the validity of this approach for studying large-scale dynamical processes and biomechanics within developing embryos.

Whole-Embryo Imaging of Native and Disrupted Morphogenetic Movements. Early *Drosophila* embryos are highly scattering for visible light and develop rapidly, which limits their direct observation using conventional imaging techniques. In contrast, 2PEF microscopy is well adapted to complex tissue observation (25–27). We performed long-term whole-embryo 4D (i.e., time-lapse 3D) imaging of appropriate GFP systems to characterize morphogenetic movements after laser-induced ablations. Imaging and ablations were performed by using the same laser source, by simply changing the average laser power and scanning speed. We could record high resolution (0.4 μm $\times$ 2 μm) images of nuclei within developing embryos over a half-hemisphere for several hours (Fig. 3 and Movie 2, which is published as supporting information on the PNAS web site) with no effect on the survival rate. Embryo opacity at stages 5–7 prevents 2PEF imaging through the entire egg. However, because morphogenetic movements are symmetrical with respect to the equatorial plane (anteroposterior, dorsoventral axis), they all occur within the accessible volume of view. Micrometer-resolution 3D mapping of all morphogenetic movements occurring simultaneously within the entire embryo is thus possible, which is of critical interest to address dynamic mechanical issues. This approach allows a direct, *in vivo* understanding of the complex native or disrupted movements and their quantification by velocimetric analysis.

Quantified Modulation of Morphogenetic Movements *in Vivo*. We took advantage of the 3D confinement of femtosecond pulse-induced ablations to locally modify the embryo structural integrity, resulting in a modulation of morphogenetic movements. We studied the influence of dorsal ablation sites on the disruption of morphogenetic movements through the whole embryo. Dissections were performed during cellularization at different locations in sGMCA embryos, and pairs of images (at the equator and near the

surface) were recorded every 30 s for 60 min to follow the resulting cell movements. Microdissections (50–100 μm long, 15–40 μm deep) were performed at the limit between regimes 3 and 4 (see Fig. 1), inducing the formation of ≈5- to 6-μm-diameter bubbles. These conditions compromised cell integrity within the targeted region but prevented long-distance shock waves that could damage surrounding structures.

To provide a μm-scale quantitative description of morphogenetic movements *in vivo*, instantaneous velocity fields were estimated from image sequences by using PIV analysis (16)(see *Methods*), a technique routinely used in fluid dynamics with recent applications to biology (4, 28). This method relies on correlation calculations and can extract velocity fields even when moving structures are not clearly defined in the images. We adapted PIV analysis to the micrometer-scale quantitative description of morphogenetic movements (see Movie 3, which is published as supporting information on the PNAS web site).

In an intact embryo (see Movie 2), a short dorsal contraction occurs at the onset of gastrulation and is directly followed by ventral furrow invagination (white arrows in Fig. 3) and cephalic furrow formation (between gray arrows in Figs. 3 and 4). Then, lateral cell movements toward the ventral part of the embryo (Fig. 4*a2*) result in ventral furrow closure and germ band convergent extension (29). A dorsal dissection in the middle part of the embryo ("mid-dorsal ablation," 40–60% egg length, Fig. 4*b1*) results in the disruption of both cephalic furrow formation and lateral cell motions (Fig. 4*b2*), preventing ventral furrow closure and disrupting germ band convergent extension. Furthermore, if a dorsal dissection is performed in the posterior part of the embryo (postdorsal ablation, 20–40% egg length, Fig. 4*c1*), cephalic furrow formation occurs normally whereas lateral cell motions are disrupted (Fig. 4*c2*). Smaller targeted areas result in spatially restricted disruption of these movements (not shown).

These results show that multiphoton ablations can be used to precisely modulate, *in vivo*, specific morphogenetic movements in wild-type embryos. The observed modulation could be induced by several mechanisms: (*i*) heating (30); (*ii*) morphogene signaling; (*iii*) removal of motor movements areas; and (*iv*) perturbation of the global mechanical state of the embryo. Based on our experiments on cellularization (Fig. 2), heating should be ruled out as a significant contribution at large distances. In addition, the observed rapid (<10 min) disruption of morphogenetic movements at large distances (>200 μm) is better accounted for by mechanical perturbations than by diffusion-dependent signaling. A more likely modulation mechanism is that the ablation of a specific area disrupts morphogenetic movements mechanically coupled to this area. First, motor regions might be locally removed by the ablation. For instance, dorsal genes play a critical motor role in the generation of the germ band extension (29, 31), such that the ablation of the most dorsal cells can directly affect this movement. Second, local ablations may perturb the mechanical integrity of the embryo. For example, extension movements cannot originate from or propagate through void areas, which can account for the observed rapid perturbations at large distances. The dependence of the observed modulation of morphogenetic movements on the precise ablation site further suggests that mechanisms *iii* and *iv* play essential roles.

Cell Movements and Twist Expression. Having shown that targeted ablations modulate specific movements, we now focus on the issue of the mechano-sensitive expression of the *twist* gene in the stomodeal primordium (SP) during *Drosophila* development (5). The *twist* gene is one of the fundamental genes of *Drosophila* early development, being involved in dorsoventral polarization and active cell deformations, as well as in the anterior gut track formation (32, 33). It was recently proposed that the expression of *twist* in SP cells is in turn modulated by cell deformations associated with morphogenetic movements (5). Until now, however, the precise mechanical behavior of SP cells during gastrulation remained incompletely understood due to a lack of appropriate techniques.

Velocimetric analysis of 2PEF image sequences was used to quantify tissue movements at the anterior pole in intact and ablated embryos (Fig. 5). In an intact embryo (Stage 6, Fig. 5*b Left*), ventral cells at the anterior pole exhibit a forward-direct movement during the 10–15 min of ventral furrow formation, with a peak velocity of 2.5 μm/min (Fig. 5*c*). After ventral furrow closure, this movement is followed by a backward-directed movement lasting 10–15 min, with a peak velocity of 3.5 μm/min, concurrent to anterior midgut invagination and germ band extension. Moreover, divergence analysis of velocimetric fields provides an estimate of the field of mean 2D local tissue deformations, as illustrated in Fig. 5*b*. This analysis indicates that the differential of the velocity fields between the dorsal and ventral side of the anterior pole results in an expansion followed by a compression of SP cells. In contrast, after a middorsal ablation (Fig. 4*b*), SP cell motions and deformations are affected (Fig. 5*b Right*): the compression movement is suppressed during the same period, concomitant with the loss of ventral furrow closure. Instead, SP cells exhibit a backward-directed movement lasting ≈25 min, with a peak velocity of 2 μm/min (Fig. 5*c*). Fig. 5 *b* and *c* indicates that the specific deformation of anterior pole cells probably results from complex tissue movements involving the ventral side of the embryo rather than from a simple compression propagating through dorsal tissue, as previously suggested by static observations (5). These deformation patterns clearly correlate with the pattern of Twist expression. After the above-described movements and anterior midgut invagination in an intact embryo (stage 7), Twist expression is strong in SP cells (see Fig. 5*d*). In contrast, after a middorsal ablation and subsequent perturbation of cell

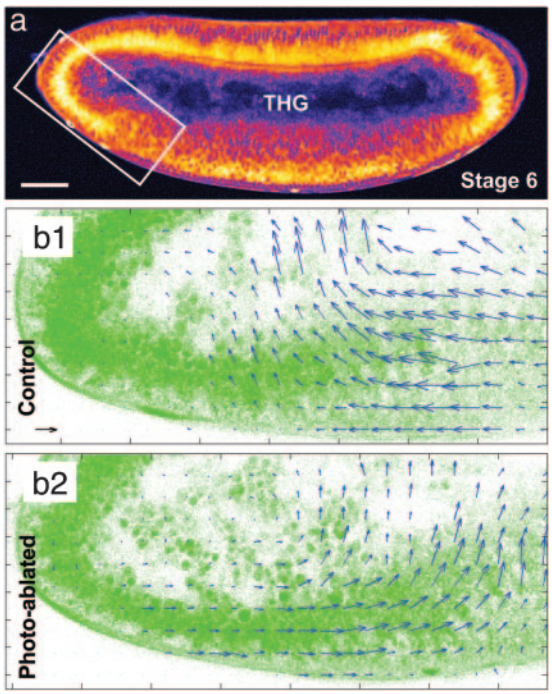

Fig. 6. Quantitative description of morphogenetic movements can be obtained in unstained embryos by using THG microscopy. (*a*) THG equator image of an unlabeled wild-type embryo (1,180-nm excitation). (Scale bar: 50 μm.) (*b1* and *b2*) Velocimetric analysis of morphogenetic movements at the anterior pole in an intact wild-type embryo (*b1*, control) and a wild-type embryo after middorsal ablation (*b2*, photoablated) observed in THG microscopy. THG image analysis provides information similar to GFP systems (see Fig. 5) in the nuclei regions, and additional information about internal structures dynamics. Data were recorded at stage 6 of development. (Black scale arrow: 3 μm/min.)

deformation at the anterior pole, Twist expression is only residual in SP cells (Fig. 5*d*).

Interestingly, we observed no significant changes in Twist expression in other regions of photo-ablated embryos compared with intact embryos at the same stage of development, which suggests that the loss of Twist expression in SP cells is linked to the disruption of the mechanical behavior rather than to any other photo-induced effect. We stress that such characterization of specific cell deformations will be of utmost importance to address the issue of mechanotransduction.

Generalization to Unlabeled Embryos Using THG Microscopy. The above-described methodology should be considered complementary to a genetic approach for studying morphogenetic movements. As such, it is necessary to extend it to unlabeled organisms, because fluorescence labeling is more difficult to obtain in mutants and, moreover, can introduce unwanted perturbations. We investigated the use of THG microscopy for characterizing native and disrupted morphogenetic movements. THG microscopy (11) was recently proposed as a general purpose imaging technique that provides 3D resolution comparable with that of 2PEF or second harmonic generation microscopy. However it has the distinct property of providing maps of optical heterogeneities from virtually any unstained transparent biological sample (34, 35).

We combined THG imaging with multiphoton ablation and 2PEF imaging (see *Methods*), and we extended THG microscopy to the quantitative imaging of morphogenetic movements in opaque unstained embryos. THG microscopy is sensitive to micrometer-size optical heterogeneities (36) and provides rich structural information from all regions within unstained embryos (Fig. 6*a* and Movie 4, which is published as supporting information on the PNAS web site). In particular, a strong signal is obtained from lipid droplets present around the nuclei, and from the interfaces of yolk structures. As such, THG images are ideally suited for velocimetric analysis (Fig. 6*b*). An additional benefit is that THG microscopy performs well deep within *Drosophila* embryos owing to the reduced scattering of excitation wavelengths in the 1,100- to 1,300-nm range, and reveals details about unstained inner structures that are not accessible with other techniques. As is apparent in Fig. 6*b*, velocimetric THG data provide simultaneous information about the dynamics of tissue and yolk internal structures and reveal their continuity. In the context of early embryo biomechanics, these data indicate that long-range mechanical coupling might propagate through the yolk as well as through the tissues. The combination of multiphoton ablation and THG microscopy is therefore a versatile method to modulate and analyze morphogenetic movements within unlabeled organisms.

In conclusion, we have shown that an all-optical approach can be used both to locally disrupt the structural integrity of tissues inside live embryos, and to quantitatively analyze the resulting immediate modulation of distant morphogenetic movements within the entire embryo over extended periods of time. This modulation is found to depend on ablation size and localization, which suggests that femtosecond laser pulse-induced ablation may allow the precise modulation of several morphogenetic movements *in vivo*. This approach brings insight into the mechanical control of morphogenesis by providing a precise description of tissue movements and deformations. Examining the interplay between *in vivo* cell deformations and molecular signals will open up many possibilities for the study of embryo development, including in organisms for which mutants exhibiting disrupted morphogenetic movements are not available. This methodology not only constitutes a complementary alternative to genetics for the study of morphogenesis, but also could be used to analyze mutant phenotypes and is more generally applicable to study other processes of development. For example, induction centers could be inactivated *in vivo* by 3D-confined submicrometer ablations, before monitoring the dynamics of subsequent embryo development using the methods demonstrated here. The combination of multimodal nonlinear microscopy with femtosecond-pulse-induced microdissection is generally applicable to other organisms and should lend itself to a wealth of additional applications in developmental biology.

We thank C. Schaffner, M. Bierry, J.-M. Sintes, and X. Solinas for technical assistance; M.-C. Schanne-Klein, N. Dostatni, J. Ogilvie, and C. Py for critical comments; D. P. Kiehart and R. A. Montague for the gift of the sGMCA transgenic line; and J. K. Sveen for providing his MATPIV package. This work was supported by the Association pour la Recherche sur le Cancer, the Délégation Générale pour l'Armement, and Institut Universitaire de France.

1. Solnica-Krezel, L. & Eaton, S. (2003) *Development (Cambridge, U.K.)* **130,** 4229–4233.
2. Keller, R., Davidson, L. A. & Shook, D. R. (2003) *Differentiation* **71,** 171–205.
3. Brouzés, E. & Farge, E. (2004) *Curr. Opin. Genet. Dev.* **14,** 367–374.
4. Hove, J. R., Köster, R. W., Forouhar, A. S., Acevedo-Bolton, G., Fraser, S. E. & Gharib, M. (2003) *Nature* **421,** 172–177.
5. Farge, E. (2003) *Curr. Biol.* **13,** 1365–1377.
6. König, K., Krauss, O. & Riemann, I. (2002) *Opt. Express* **10,** 171–176.
7. Joglekar, A. P., Liu, H.-H., Meyhöfer, E., Mourou, G. & Hunt, A. J. (2004) *Proc. Natl. Acad. Sci. USA* **101,** 5856–5861.
8. Vogel, A., Noack, J., Nahen, K., Theisen, D., Bush, S., Parlitz, U., Hammer, D. X., Noojin, G. D., Rockwell, B. A. & Birngruber, R. (1999) *Appl. Phys. B* **68,** 271–280.
9. Tirlapur, U. K. & König, K. (2002) *Nature* **418,** 290–291.
10. Denk, W., Strickler, J. H. & Webb, W. W. (1990) *Science* **248,** 73–76.
11. Barad, Y., Eisenberg, H., Horowitz, M. & Silberberg, Y. (1997) *Appl. Phys. Lett.* **70,** 922–924.
12. Davis, I., Girdham, C. H. & O'Farrell, P. H. (1995) *Dev. Biol.* **170,** 726–729.
13. Kiehart, D. P., Galbraith, C. G., Edwards, K. A., Rickoll, W. L. & Montague, R. A. (2000) *J. Cell Biol.* **149,** 471–490.
14. Wieschaus, E. & Nusslein-Volhard, C. (1998) in *Drosophila*: *A Practical Approach* (Oxford Univ. Press, Oxford), pp. 179–214.
15. Xu, C., Zipfel, W., Shear, J. B., Williams, R. M. & Webb, W. W. (1993) *Proc. Natl. Acad. Sci. USA* **93,** 10763–10768.
16. Raffel, M., Willert, C. & Kompenhans, J. (1998) *Particle Image Velocimetry*: *A Practical Guide* (Springer, Berlin).
17. Oehring, H., Riemann, I., Fischer, P., Halbhuber, K.-J. & König, K. (2000) *Scanning* **22,** 263–270.
18. König, K., Becker, T., Fischer, P., Riemann, I. & Halbhuber, K. (1999) *Opt. Lett.* **24,** 113–115.
19. Galbraith, J. A. & Terasaki, M. (2003) *Mol. Biol. Cell* **14,** 1808–1817.
20. Tsai, P. S., Friedman, B., Ifarraguerri, A. I., Thompson, B. D., Lev-Ram, V., Schaffer, C. B., Xiong, Q., Tsien, R. Y., Squier, J. A. & Kleinfeld, D. (2003) *Neuron* **39,** 27–41.
21. Royou, A., Field, C., Sisson, J. C., Sullivan, W. & Karess, R. (2004) *Mol. Biol. Cell* **15,** 838–850.
22. Thomas, J. H. & Wieschaus, E. (2003) *Development (Cambridge, U.K.)* **131,** 863–871.
23. Schönle, A. & Hell, S. (1998) *Opt. Lett.* **23,** 325–327.
24. Schaffer, C., Garcia, J. & Mazur, E. (2003) *Appl. Phys. A* **76,** 351–354.
25. Zipfel, W. R., Williams, R. M. & Webb, W. W. (2003) *Nat. Biotechnol.* **21,** 1369–1377.
26. Squirrell, J. M., Wokosin, D. L., White, J. G. & Bavister, B. D. (1999) *Nat. Biotechnol.* **17,** 763–767.
27. Charpak, S., Mertz, J., Beaurepaire, E., Moreaux, L. & Delaney, K. (2001) *Proc. Natl. Acad. Sci. USA* **98,** 1230–1234.
28. Py, C., de Langre, E., Hémon, P., Moulia, B. & Doaré, O. (2004) in *Flow-Induced Vibrations VIII*, eds. de Langre, E. & Axisa, F. (Ecole Polytechnique, Palaiseau, France), Vol. 2, pp. 155–160.
29. Costa, M., Sweeton, D. & Wieschaus, E. (1993) in *The Development of Drosophila melanogaster* (Cold Spring Harbor Lab. Press, Plainview, NY), pp. 425–465.
30. Jack, R. S., Gehring, W. J. & Brack, C. (1981) *Cell* **24,** 321–331.
31. Roth, S., Hiromi, Y., Godt, D. & Nusslein-Volhard, C. (1991) *Development (Cambridge, U.K.)* **112,** 371–388.
32. Jiang, J., Kosman, D., Ip, Y. T. & Levine, M. (1991) *Genes Dev.* **5,** 1881–1891.
33. Reuter, R., Grunewald, B. & Leptin, M. (1993) *Development (Cambridge, U.K.)* **119,** 1135–1145.
34. Yelin, D. & Silberberg, Y. (1999) *Opt. Express* **5,** 196–175.
35. Chu, S.-W., Chen, S.-Y., Tsai, T.-H., Liu, T.-M., Lin, C.-Y., Tsai, H.-J. & Sun, C.-K. (2003) *Opt. Express* **11,** 3093–3099.
36. Cheng, J.-X. & Xie, X. S. (2002) *J. Opt. Soc. Am. B* **19,** 1604–1610.